HYDROGEN, FUEL CELL & ENERGY STORAGE

A new SEPIC-Zeta bidirectional converter with high efficiency for renewable energy systems

Akram Qasim Kadhim Almohammed[a] | **Majid Delshad**[a,b,*] | **Nasseer Kassim Bachache**[c] | **Bahador Fani**[a] | **Hadi Saghafi**[a]

[a] Department of Engineering, Isfahan (Khorasgan) Branch, Islamic Azad University, Isfahan, Iran
[b] Département de Génie Électrique, École de Technologie Supérieure, Montréal, QC, H3C 1K3, Canada
[c] Department of Power Electrical Engineering Techniques, Bilad Alrafidain University College, Iraq
[*] Corresponding author, Email: delshad@khuisf.ac.ir

Article Information

Article Type
Research Article

Article History
Received: *10 Jun 2024*
Revised: *05 Aug 2024*
Accepted: *01 Sep 2024*
Published Online: *04 Sep 2024*

Keywords
Bidirectional converter
Soft switching
SEPIC converter
High efficiency
ZVT

Abstract

This study introduces a new bidirectional converter that maintains the zero-voltage switching feature without complicating the circuit operation through an auxiliary circuit. Additionally, the circuit's design ensures consistent operation during both ascending and descending modes, coupled with a straightforward control circuit. An exhaustive analysis of the converter in various modes has been performed. Furthermore, the converter operates symmetrically in both step-up and step-down modes, with two out of the four switches remaining off in each mode. The auxiliary circuit introduced in this design is a model of modularity and versatility. It seamlessly integrates with two-phase or multi-phase bidirectional converters without necessitating extra components. Imagine it as a universal adapter that, regardless of the number of phases or the direction of conversion, plugs in effortlessly, enhancing the system's functionality without cluttering it with additional parts. This innovative approach not only simplifies the design process but also streamlines the overall architecture, making it a highly efficient solution for complex power conversion scenarios. Simulation of the proposed converter was conducted using PSPICE software, validating the theoretical analysis. Furthermore, a 60 W prototype of the converter was constructed, which its outcomes corroborated the simulation findings.

Cite this article: Almohammed, A. Q. K., Delshad, M., Bachache, N. K., Fani, B., Saghafi, H. (2024). A new SEPIC-Zeta bidirectional converter with high efficiency for renewable energy systems. DOI: 10.22104/HFE.2024.6809.1292

 Publisher: Iranian Research Organization for Science and Technology (IROST)
DOI: 10.22104/HFE.2024.6809.1292

1 Introduction

To address environmental pollution and the depletion of fossil fuels, electricity generation is increasingly relying on renewable energy sources (RES). However, the dependability of RES is significantly compromised due to the variable and intermittent nature of their power output. To enhance reliability, energy storage devices (ESD) like batteries and supercapacitors are employed [1]. Particularly, supercapacitors, which exhibit lower voltage levels, necessitate a power electronic interface to match the 3-phase, 400 V rms load voltage, requiring at least a 600 V dc-link voltage. In such scenarios, a non-isolated boost converter is often used to amplify the voltage gain. Yet, the primary challenges with boost converters are their limited voltage transfer ratio (VTR) and the elevated voltage stress on the semiconductor components [2]. To address these limitations, literature has introduced high-gain converters leveraging concepts such as Switched Capacitor (SC), Switched Inductor (SL), Voltage Multiplier (VM), among others [3].

Numerous high-gain dc-dc converters have been documented, derived from these concepts, yet they are not capable of bidirectional operation [4]. Boosting low-voltage batteries directly with a high-voltage conversion ratio (VCR) bidirectional DC-DC converter presents an alternative strategy. Among various options, the Dual Active Bridge (DAB) converter is a favored choice for enabling bidirectional power flow within isolated configurations [5]. Its VCR can be flexibly modified by altering the transformer's turn ratio. While the voltage-fed DAB features a straightforward design and high power density, it suffers from high input current ripple. However, its operational limitations within a broad VCR range, due to constrained zero voltage switching (ZVS) capabilities and increased circulation losses, make it less suited for wide-ranging applications [6, 7]. Attempts to address these challenges by integrating additional switches or transformers have resulted in increased circuit and control complexity [8].

Current-fed DAB variants, capable of achieving ZVS across a wide voltage spectrum, necessitate extra DC inductors, thus diminishing power density. In various scenarios, particularly those not requiring galvanic isolation like hybrid electric vehicle (HEV) motor drives, DC microgrid energy storage systems, and more, nonisolated DC-DC converters offer a viable solution [9, 10]. These converters generally boast higher power density and cost-effectiveness compared to their isolated counterparts. Despite the conventional buck/boost converter's theoretical capability for bidirectional high VCR, practical limitations arise due to the inductor's equivalent series resistance (ESR), diminishing voltage gain at high duty cycles [11]. The selection of suitable switches becomes challenging due to equivalent high voltage stress and peak inductor current, thereby reducing conversion efficiency [12,13]. As a result, the high-voltage side (HVS) typically does not exceed four times the low-voltage side (LVS). A proposed solution involves a two-stage buck/boost cascade topology, achieving a squared VCR of the traditional buck/boost converter with just four switches, although this necessitates the use of high-voltage rated switches due to ZVS losses in some cases [14].

Alternative topologies employing coupled inductors can achieve high VCRs by adjusting the turns ratio but face issues like voltage spikes and electromagnetic interference upon switch deactivation, alongside challenges in achieving consistent coupling coefficients for mass production. Switched capacitor converters, noted for their straightforward cascaded structure and high power density, mainly derive their VCR from the capacitor count, limiting their modulation by duty cycle and suitability to fixed-source voltage applications [15]. Integrating the switched capacitor structure into boost circuits has been explored to modulate HVS voltage via duty cycle and enhance VCR with fewer capacitors, though most research focuses on unidirectional power flow. Bidirectional high VCR converters have seen limited discussion, with existing models like the series capacitor buck converter and multistage bidirectional topology necessitating complex designs or additional components to manage voltage spikes and ensure ZVS, ultimately requiring high-voltage rated switches [16]. The bidirectional SEPIC-Zeta converters offer advantages over DAB converters, such as having fewer switches and a faster dynamic response [17, 18].

This research introduces a new bidirectional SEPIC-Zeta converter characterized by a symmetrical auxiliary circuit and straightforward operation. It ensures zero voltage switching (ZVS) conditions for the circuit switches, significantly reducing the converter's losses. Moreover, the converter operates symmetrically in both step-up and step-down modes, utilizing only two of its four switches in either mode.

In this study, a bidirectional converter is to be introduced, and its performance in both step-up and step-down modes is to be examined in section 2. In section 3, an extensive analysis of the proposed converter is to be conducted, involving the derivation of design equations for its components and the calculation of voltage stress on semiconductor elements. To validate the theoretical analysis of the proposed converter, a simulation was conducted using PS software, with the results detailed in section 4. Additionally, a 60 W prototype was constructed, and the practical outcomes are examined in

section 5. Finally, the conclusion is presented in section 6.

2 The proposed convertor

The proposed bidirectional converter, illustrated in Figure 1, operates in two modes: step-up and step-down. The design comprises two segments: the primary circuit, which contains switches M_1 and M_3, an inductor L, and a capacitor C, and the auxiliary circuit, which includes coupled inductors L_1-L_2, switches M_2-M_4, capacitors C_1 and C_2, diodes D_{a1} and D_{a2}, a snubber capacitor C_M, and a resonant inductor L_r. Commands are given to switches M_1 and M_2 during step-up mode and to switches M_3 and M_4 in step-down mode.

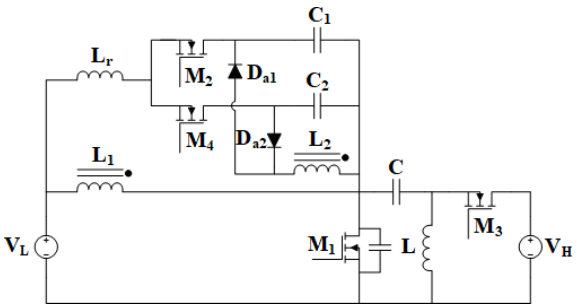

Fig. 1. The proposed SEPIC-Zeta bidirectional converter.

In step-up mode, the converter operates through four distinct stages within a single switch cycle. During this mode, switches M_1 and M_2 are signaled, while switches M_3 and M_4 remain inactive. For simplicity in analyzing the circuit, the voltages across capacitors C, C_0, C_1, and C_2 are presumed constant, and the inductors' current is disregarded. Prior to the commencement of the first interval, M_1 is deactivated with the body diode of M_3 (D_{M3}) conducting, allowing the inductor L to discharge into the output. Figure 2 shows the key waveforms of the step-up mode and Figure 3 illustrates the equivalent circuit of the converter in each mode.

2.1 Operation in step-up mode

The First Interval This interval initiates with the activation of switch M_2. A resonance between L_r and capacitor C_{M1} occurs, leading to the discharge of the capacitor. Once fully discharged, the body diode of M_1 conducts, signaling the end of this interval.

The Second Interval Upon the body diode of M_1 conducting, switch M_1 can be activated under Zero Voltage (ZV) conditions. During this interval, as the constant reverse voltage across L_r diminishes, the current through M_2 linearly decreases, alongside the body diode current, until the current shifts from the body diode of M_1 to M_1 itself. The interval concludes once the switch current equals I_{Lm1}, deactivating diode D_{M3}.

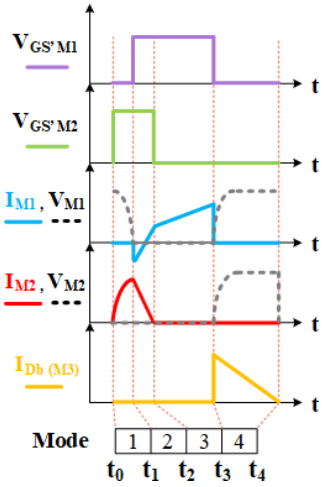

Fig. 2. The keywaveform of the proposed bidirectional converter in step-up mode.

The Third Interval Following the deactivation of D_{M3}, the charging of L_{M1} occurs linearly. Concurrently, switch M_2 is turned off under Zero Voltage Zero Current (ZVZC) conditions. During this period, Co fulfills the load current requirement. This interval concludes with the deactivation of M_1.

The Fourth Interval With the deactivation of M_1, the body diode D_{M3} conducts, initiating the discharge of inductor L into the output. Here, the auxiliary circuit is disengaged from the converter. This interval wraps up with the reactivation of M_2.

2.2 Operation in step-down mode

Similar to the step-up mode, the converter in step-down mode progresses through four intervals within a switch cycle, with commands directed to switches M_3 and M_4 while switches M_1 and M_2 remain inactive. In this scenario, switch M_4 is activated before M_3, discharging the capacitor M_3 and establishing Zero Voltage (ZV) conditions for the switch. The same initial conditions applied to step-up mode are assumed here.

The First Interval This interval initiates with switch M_4 being turned on, causing a resonance between L_r and the input capacitor of M_3, leading to the discharge of M_3's capacitor and the conduction of M_1's body diode. From this point, M_3 can be activated under ZV conditions.

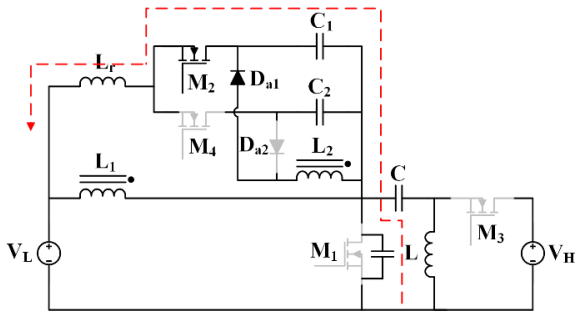

(a) Interval 1.

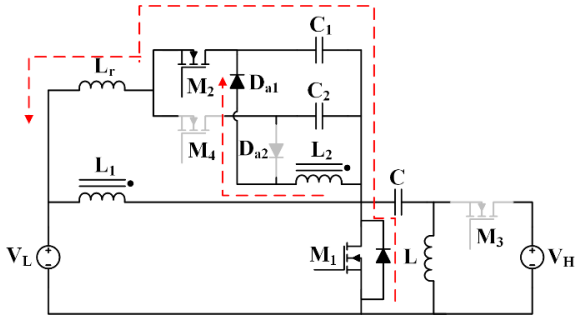

(b) Interval 2.

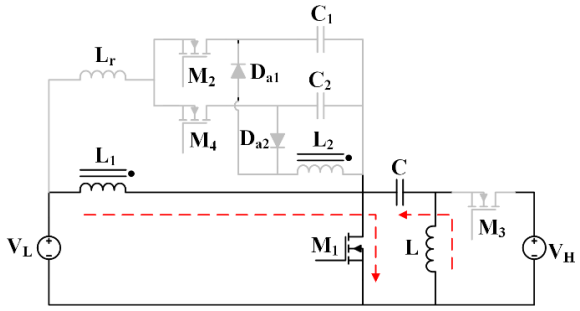

(c) Interval 3.

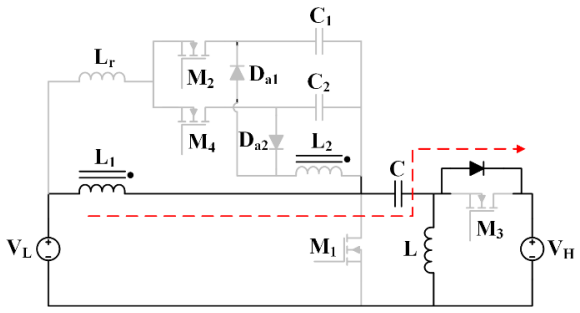

(d) Interval 4.

Fig. 3. The equaivalent circuits of the proposed converter in step-up mode.

The Second Interval Following the deactivation of D_{M1}, the voltage across L_r drops, and the current through M_4 decreases linearly until it reaches zero, allowing it to be turned off under Zero Current (ZC) conditions. Simultaneously, the current through D_{M3} decreases until it shifts from D_{M3} to M_3, increasing to I_{Lm1} level and marking the end of this interval.

The Third Interval With D_{M1} is turned off, inductor L is charged through V_H, and the energy from capacitor C is discharged into the output.

The Fourth Interval Upon M_3's deactivation, the capacitor of M_3 charges, and inductor L begins discharging into the output. In this mode, M_4 is turned off under ZVZC conditions, removing the auxiliary circuit from the converter entirely.

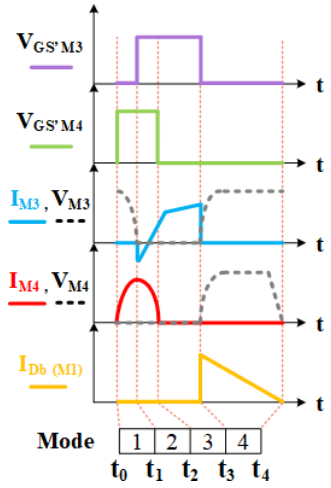

Fig. 4. The keywaveform of the proposed bidirectional converter in step-down mode.

3 Analysis of the proposed bidirectional convertor

In this section, both the converter's gain and the specifics for designing its components are discussed. During step-down operation, the output voltage, is given by the equation $V_L = \frac{DV_H}{1-D}$, where V_H is the input high voltage and D is the duty cycle. Consequently, the voltage across capacitor C_2 can be determined using a similar approach. Likewise, the voltage across capacitor C_1 is derived following the same principle.

$$V_{C_2} = n(1-D)V_L = nDV_H\,, \tag{1}$$

$$V_{C_1} = nV_L = \frac{nD}{1-D}V_H\,, \tag{2}$$

$$\frac{V_L}{V_H} = \frac{D}{1-D}\,, \tag{3}$$

$$V_{M_1} = V_{M_3} = \frac{V_H}{D}\,, \tag{4}$$

$$V_{D_{a1}} = V_{D_{a2}} = (2-D)V_H\,, \tag{5}$$

where V_L is low voltage side and n is turn ratio of coupled-inductor L_1-L_2.

The efficiency of this converter mirrors that of a standard SEPIC converter. Figure 6 illustrates how the converter's efficiency varies with alterations in the duty cycle for both step-up and step-down operations.

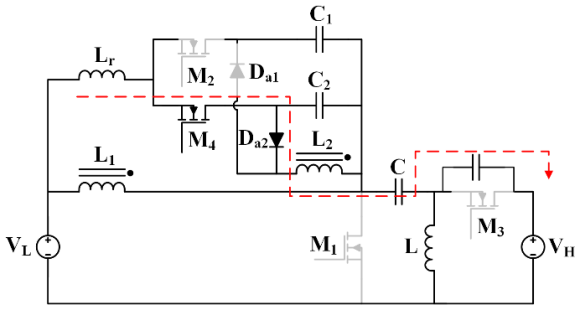

(a) Interval 1.

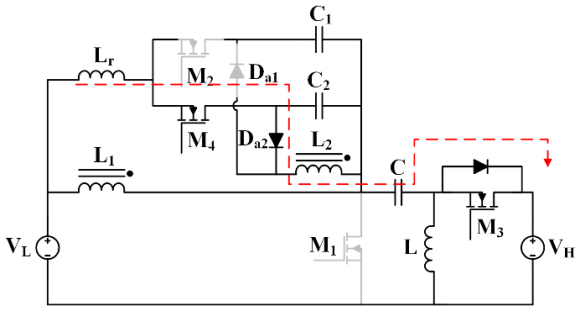

(b) Interval 2.

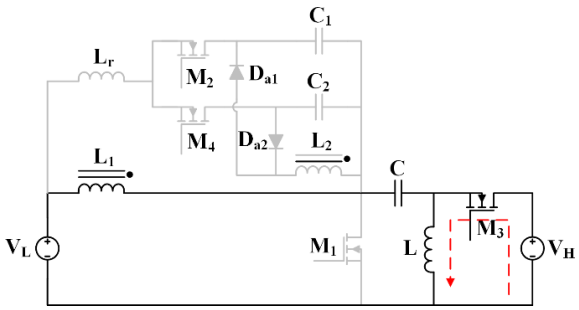

(c) Interval 3.

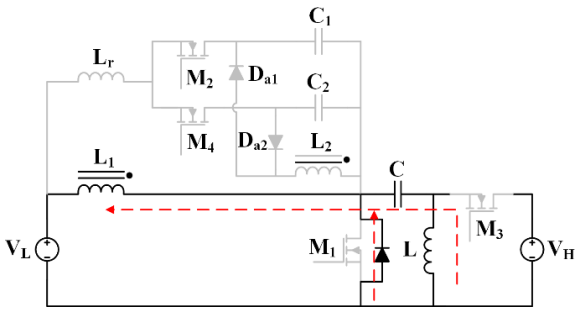

(d) Interval 4.

Fig. 5. The equaivalent circuits of the proposed converter in step-down mode.

Additionally, Figure 7 displays the normalized voltage stress exerted on the switches relative to the high voltage. Observably, voltage stress diminishes with an increase in the duty cycle, making a duty cycle of 0.5, the optimal selection for design purposes.

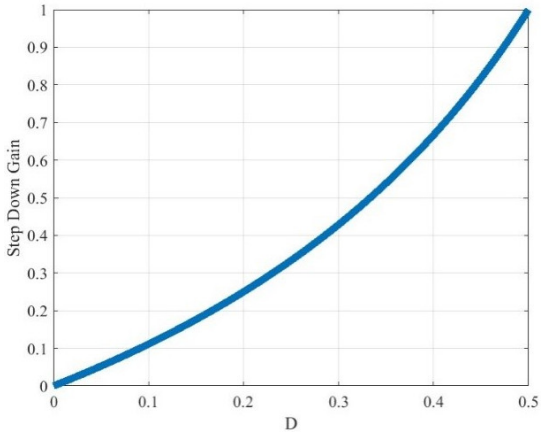

(a) Step-up mode

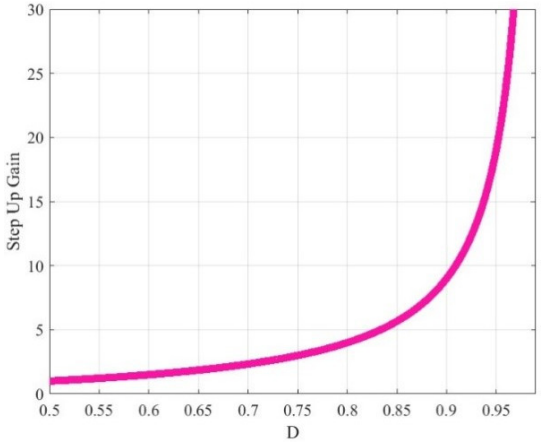

(b) Step-down mode

Fig. 6. Proposed bidirectional converter gain diagram.

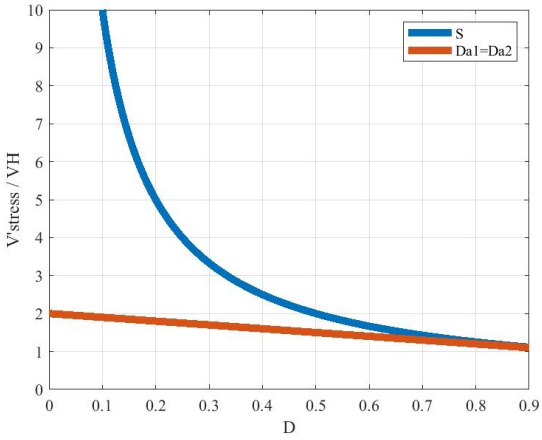

Fig. 7. Normalized elements stress diagram of suggested bidirectional converter.

4 Simulation results

To validate the theoretical analysis of the proposed converter, it was simulated for a high voltage of 110 volts, a low voltage of 48 volts, and a power of 60 W using PSpice software. The specifications of the designed components are listed in Table 1. Moreover, the schematic representation of the proposed high step-up converter simulated in both step-up and step-down modes is shown in Figure 8.

Table 1. Specifications of suggested converter and its elements values.

Elements/Specifications	Part name/Value
V_{in}	48 V
V_O	110 V
Power switch	IRF740
L_1, L_3	270 - 100 μH
Turns ratio = N	0.6
L_r	2 μH
$C_2 - C_1$	10 μF
C_o	100 μF
C_s	4.7 nF
P_O	60 W
f_S	100 kHz

The simulation outcomes in both these modes are depicted in Figures 9 to 16. Figures 9 and 10 display the current and voltage waveforms for switches M_1 and M_2 in the step-up mode. It is observed from Figure 9 that the current is negative at the instant the switch is activated, thereby turning on the body diode and facilitating zero voltage switching conditions. Similarly, as seen in Figure 10, the auxiliary switch M_2 is activated and deactivated under zero current conditions. Figure 11 illustrates that the M_3 body diode of switches at zero current, avoiding the reverse recovery issue due to the progressive increase and decrease in its current upon activation and deactivation, respectively, attributed to the leakage inductor.

In Figures 12 and 13, the current and voltage waveforms for switches M_3 and M_4 in the step-down mode are illustrated. As indicated in Figure 12, the current turns negative when switch M_3 is activated, hence the body diode is activated, providing zero voltage switching conditions. Furthermore, Figure 13 shows that the auxiliary switch M_4 is activated and deactivated under zero current conditions. According to Figure 14, the M_1 body diode switches at zero current due to the gradual increase and decrease of its current when switched on and off, respectively, due to the leakage inductance, thus avoiding any reverse recovery issues.

5 Experimental results

Figure 15 shows the implemented converter and Figure 16 presents the practical results of the proposed bidirectional converter in step-up mode, and step-down mode. As depicted in Figure 16a, when the switch is activated, the current is in the negative direction, causing M_1's body diode to conduct. Simultaneously, M_1's voltage rises at the moment it is turned off, thus facilitating the conditions for the switch's activation and deactivation. Figure 16c demonstrates that switch M_3, when in step-down mode, experiences similar conditions. The current waveform of the auxiliary switch M_2 (bottom) and M_3's body diode (top) is shown in Figure 16b, illustrating zero-current switching in both M_2 and body diode of M_3 and corroborating the simulation outcomes. Analogous conditions are observed for the auxiliary switch M_4 and body diode M_1, as shown in Figure 16d. The practical outcomes validate the simulation results and theoretical analysis of the converter. The observed unwanted fluctuations in these results stem from the resonance of the switch's internal capacitor with the leakage inductance.

5.1 Comparison of the proposed bidirectional converter efficiency in step-up and step-down modes

The efficiency of the proposed bidirectional converter in both the high step-up and high step-down modes is depicted in Figure 17. It is observed that the optimal efficiency is attained at full load. Due to the circulating current in the auxiliary circuit, a decrease in power results in reduced efficiency in both modes.

5.2 The Comparison of the proposed bidirectional converter with previous bidirectional converters

In this section, the proposed converter is compared with several recent bidirectional converters. As shown in Table 2, Converters [19] and [20] feature soft switching and low voltage stress on their components. However, they have a high number of switches, resulting in a more complex control circuit operation. Converters [21] and [22] have fewer components than the proposed converter, but Converter [21] has the problem of high current ripple, and Converter [22] lacks a common ground. Converter [23] is a bidirectional converter with high voltage gain and low voltage stress, but it also has high current ripple and lacks a common ground.

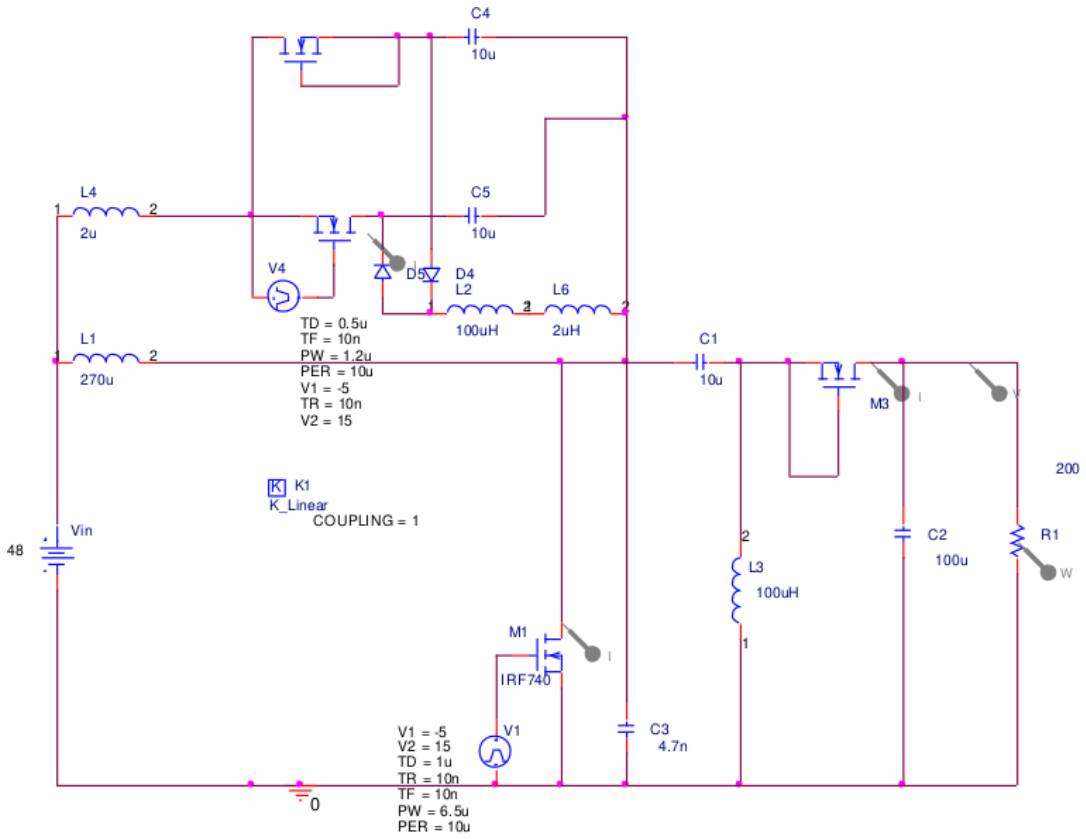

(a) step-up mode

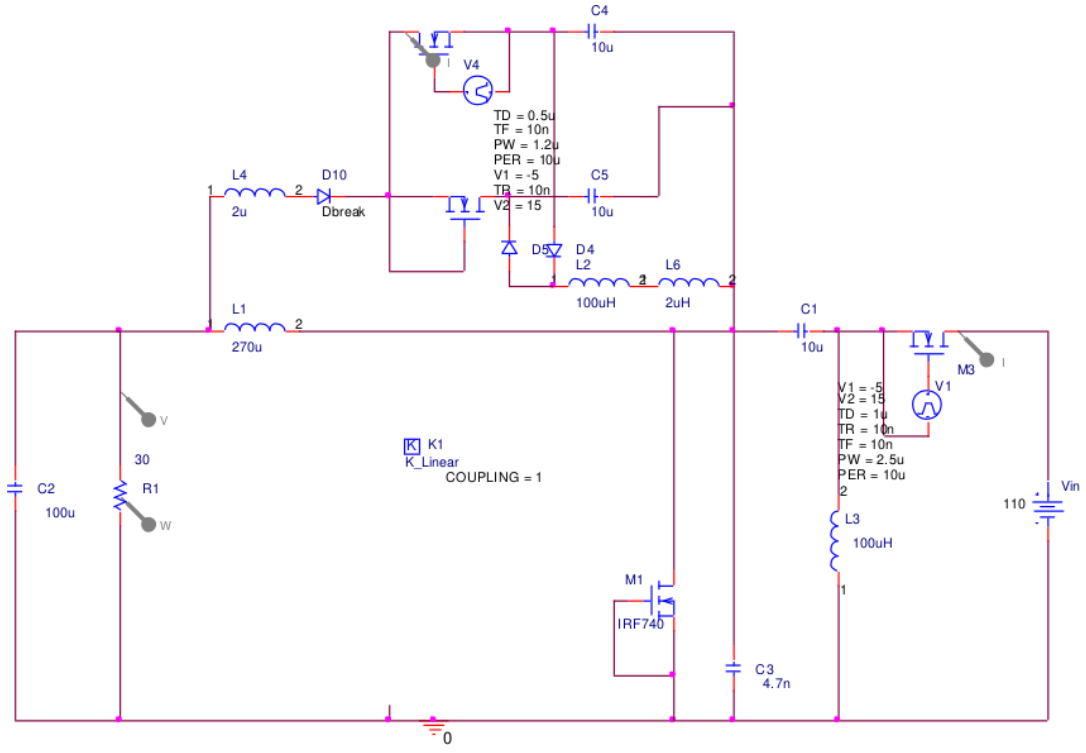

(b) step-down mode

Fig. 8. Schematic view of the proposed bidirectional converter simulated in PSpice software.

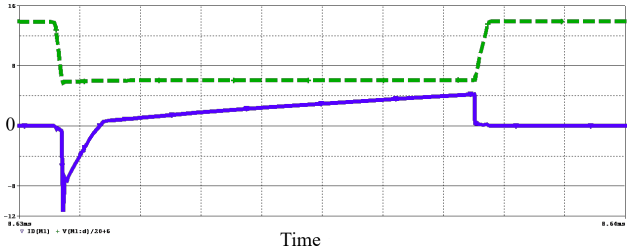

Fig. 9. Simulated converter switch M_1 current (bottom) and voltage (top) waveform in step-up mode in scale (1 μs/div, 4 A/div, 80 V/div).

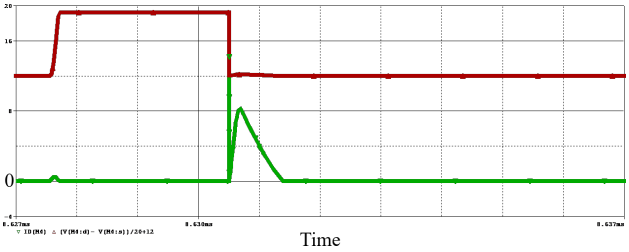

Fig. 10. Simulated converter switch M_2 current (bottom) and voltage (top) waveform in step-up mode in scale (1 μs/div, 4 A/div, 80 V/div).

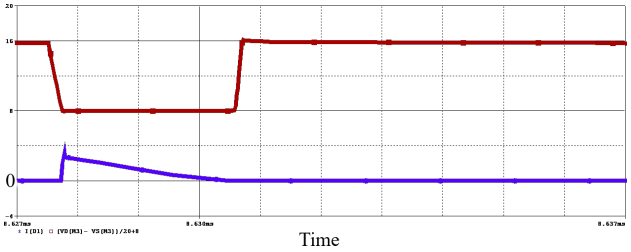

Fig. 11. Simulated converter D_{M3} current (bottom) and voltage (top) waveform in step-up mode in scale (1 μs/div, 4 A/div, 80 V/div).

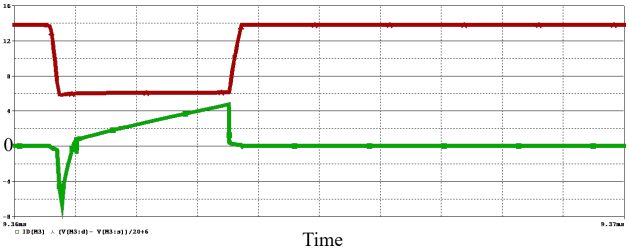

Fig. 12. Simulated converter switch M_3 current (bottom) and voltage (top) waveform in step-down mode in scale (1 μs/div, 2 A/div, 40 V/div).

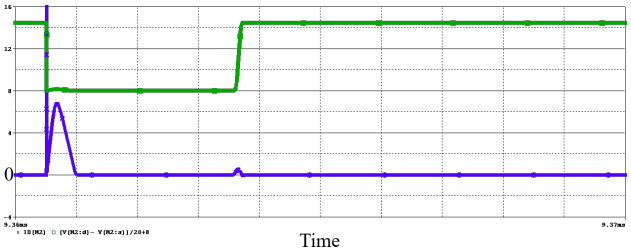

Fig. 13. Simulated converter switch M_4 current (bottom) and voltage (top) waveform in step-down mode in scale (1 μs/div, 2 A/div, 40 V/div).

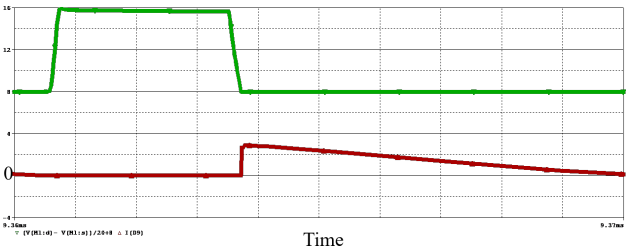

Fig. 14. Simulated converter switch D_{M1} current (bottom) and voltage (top) waveform in step-down mode in scale (1 μs/div, 2 A/div, 40 V/div).

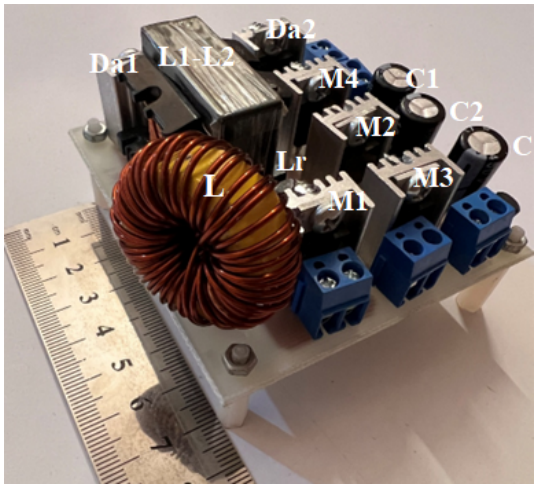

Fig. 15. The implimented proposed bidirectional converter.

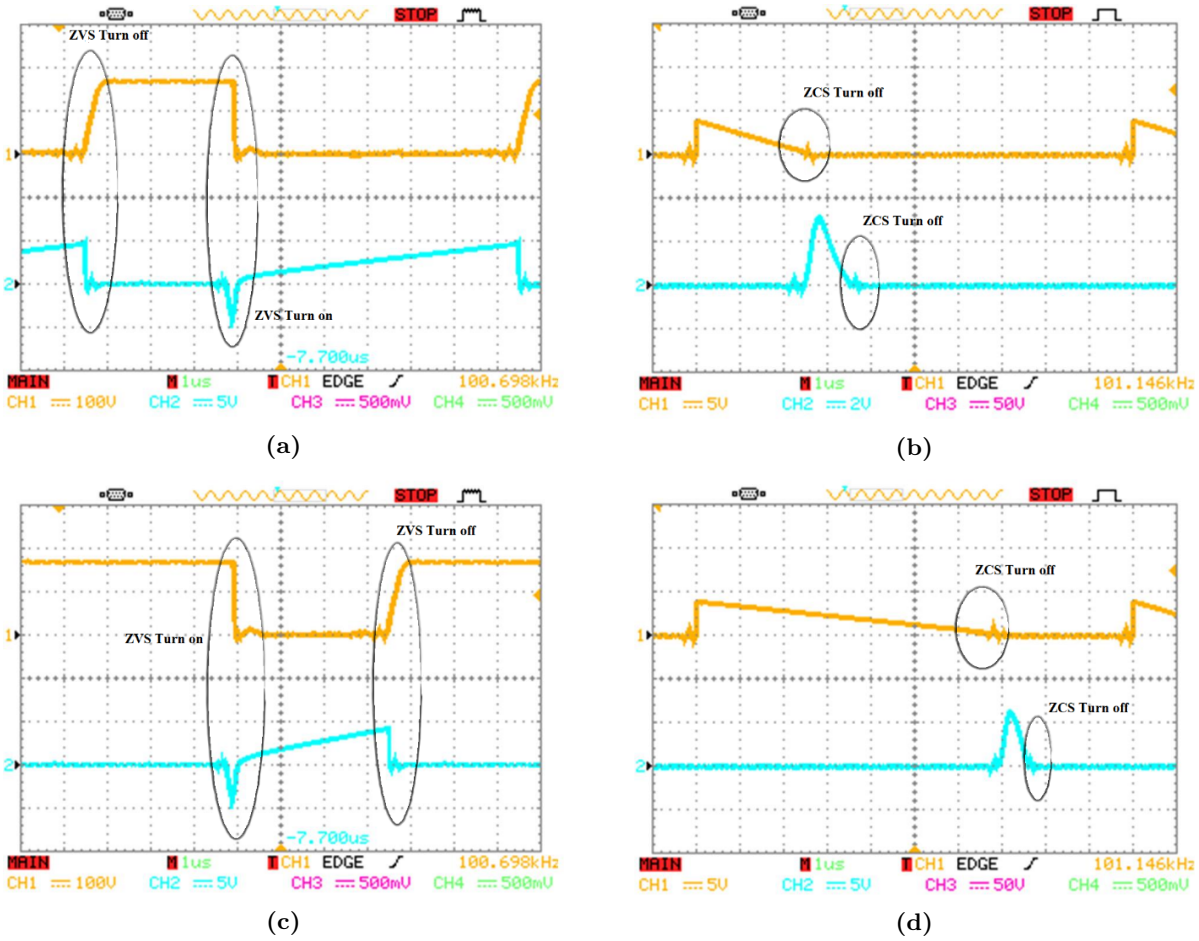

Fig. 16. The experimental results of the proposed bidirectional converter. (a) Voltage (top) and current (bottom) of the M_1 in step-up mode; (b) The current waveforms of M_2 (bottom) and body diode of M_3 (top) in step-up mode; (c) Voltage (top) and current (bottom) of the M_3 in step-down mode; (d) The current waveforms of M_4 (bottom) and body diode of M_1 (top) in step-down mode (100 V/div, 5 A/div, 1 μs/div).

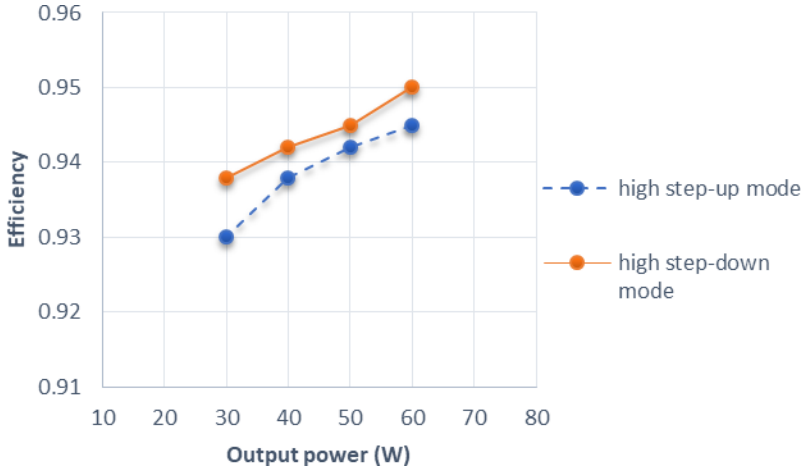

Fig. 17. Efficiency diagram of the proposed bidirectional converter in step-up and step-down modes.

Table 2. The Comparison of the proposed bidirectional converter with other convertors.

Converter	Switches Count	Control Flexibility	Soft switching	Current ripple	Common Ground	Total elements Count
[19]	7	High	Yes	Low	No	14
[20]	8	Medium	Yes	High	Yes	14
[21]	5	Medium	No	High	Yes	9
[22]	4	Low	No	Low	No	12
[23]	6	Medium	No	Low	No	13
Proposed	4	Low	Yes	Low	Yes	13

6 Conclusions

In conclusion, the proposed bidirectional converter showcases a multitude of advantages that are pivotal for its operational efficiency and effectiveness. Key among these benefits is the provision of Zero-Voltage Switching (ZVS) conditions for activating the switches, significantly diminishing switching losses and ensuring smoother transitions.

The auxiliary circuit, as a standout feature, maintains a low circulating current, thereby minimizing any potential for energy waste. This same circuit aids in switching off the body diodes under Zero-Current Switching (ZCS) conditions, effectively addressing the reverse recovery challenge, a common hurdle in power electronics. Remarkably, the auxiliary circuit accomplishes its role without inflicting noticeable losses on the converter, preserving its overall efficiency. Its modular nature allows for seamless integration into various setups without the need for additional elements, exemplifying versatility and ease of adaptation.

The implementation of Pulse Width Modulation (PWM) control simplifies the control circuit, making it straightforward to manage while eliminating capacitive turn-on losses in switches due to the ZVS feature. Furthermore, the converter is engineered to offer soft switching conditions across a broad spectrum of load variations, enhancing its reliability and performance under diverse operating conditions. One disadvantage of the proposed converter is the floating source of the auxiliary switches, which necessitates the use of isolated drivers. However, considering the presence of optocouplers, this isolation does not affect the size and cost of the drive circuit. These attributes not only underline the converter's innovative design but also its practical applicability in modern power conversion applications. To advance the research on the bidirectional converter, efforts should focus on implementing strategies to reduce current ripple and on detailed modeling for optimizing the control circuit design for enhanced performance and efficiency.

Abbreviations

ZVS	Zero Voltage Switching
ZCS	Zero Current Switching
PWM	Pulse Withd Modulation
D	Duty cycle
RES	Renewable Energy Sources
ESD	Energy Storage Devices
VTR	Voltage Transfer Ratio
SC	Switched Capacitor
SL	Switched Inductor
VM	Voltage Multiplier
VCR	Voltage Conversion Ratio
μs	Microsecond

References

[1] Karthikeyan V, Kumaravel S, Gurukumar G. High step-up gain DC–DC converter with switched capacitor and regenerative boost configuration for solar PV applications. IEEE Transactions on Circuits and Systems II: Express Briefs. 2019;66(12):2022–2026. 143

[2] Heydari-doostabad H, O'Donnell T. A wide-range high-voltage-gain bidirectional DC–DC converter for V2G and G2V hybrid EV charger. IEEE Transactions on Industrial Electronics. 2021;69(5):4718–4729. 143

[3] Ehsani M, Singh KV, Bansal HO, Mehrjardi RT. State of the art and trends in electric and hybrid electric vehicles. Proceedings of the IEEE. 2021;109(6):967–984. 143

[4] Elsayad N, Moradisizkoohi H, Mohammed OA. A new hybrid structure of a bidirectional DC-DC converter with high conversion ratios for electric vehicles. IEEE Transactions on Vehicular Technology. 2019;69(1):194–206. 143

[5] Xu G, Sha D, Zhang J, Liao X. Unified boundary trapezoidal modulation control utilizing fixed

duty cycle compensation and magnetizing current design for dual active bridge DC–DC converter. IEEE Transactions on Power Electronics. 2016;32(3):2243–2252. 143

[6] Mohammed Qasim H, Fani B, Delshad M, Heydaran-Daroogheh-Amnyieh Z. Analysis and implementation of high step-up SEPIC converter without coupled inductor for high voltage applications. Hydrogen, Fuel Cell & Energy Storage. 2023;10(3):201–213. Available from: https://hfe.irost.ir/article_1341.html. 143

[7] Tohidi B, Delshad M, Saghafi H. A new interleaved zvt high step-up converter with low count elements for photovoltaic applications. Journal of Renewable Energy and Environment. 2022;9(1):70–77. 143

[8] Vesali M, Delshad M, Adib E, Amini MR. A new nonisolated soft switched DC-DC bidirectional converter with high conversion ratio and low voltage stress on the switches. International Transactions on Electrical Energy Systems. 2021;31(1):e12666. 143

[9] Es-Haghpour I, Delshad M, Javadi S. A new interleaved ZVT high step-up converter with low input current ripple. International Journal of Electronics. 2022;109(11):1935–1953. 143

[10] Rai RK, Dixit A, Pundhir S, Peter J. Advanced integrated bidirectional ac/dc and dc/dc converter for plug-in hybrid electric vehicles. In: 2020 International Conference on Futuristic Technologies in Control Systems & Renewable Energy (ICFCR). IEEE; 2020. p. 1–6. 143

[11] Uno M, Sugiyama K. Switched capacitor converter based multiport converter integrating bidirectional PWM and series-resonant converters for standalone photovoltaic systems. IEEE Transactions on Power Electronics. 2018;34(2):1394–1406. 143

[12] Mohammadi MR. A lossless turn-on snubber for reducing diode reverse recovery losses in bidirectional buck/boost converter. IEEE Transactions on Industrial Electronics. 2019;67(2):1396–1399. 143

[13] Chen X, Xu G, Han H, Sun Y, Su M. Dual-mode bidirectional LLC-DAB converter based on a modulated coupled inductor. IEEE Transactions on Power Electronics. 2022;38(1):90–95. 143

[14] Tang CY, Wang CW, Chien HC. A Dynamic Smooth Transition Control Integrated With Hybrid Modulation for Wide Output Voltage Range Bidirectional CLLC Resonant Converters. IEEE Transactions on Power Electronics. 2023;. 143

[15] Ragasudha C, Hemamalini S. Performance Analysis of a High Gain Bidirectional DC-DC Converter Fed Drive for an Electric Vehicle with Battery Charging Capability During Braking. IEEE Access. 2024;. 143

[16] Martinez-Vera E, Banuelos-Sanchez P. Review of Bidirectional DC-DC Converters and Trends in Control Techniques for Applications in Electric Vehicles. IEEE Latin America Transactions. 2024;22(2):144–155. 143

[17] Kim ID, Paeng SH, Ahn JW, Nho EC, Ko JS. New bidirectional ZVS PWM sepic/zeta DC-DC converter. In: 2007 IEEE International Symposium on Industrial Electronics. IEEE; 2007. p. 555–560. 143

[18] Ulrich B. Analysis of a ZVS synchronous Sepic/Zeta dc/dc converter. In: PCIM Europe 2018; International Exhibition and Conference for Power Electronics, Intelligent Motion, Renewable Energy and Energy Management. VDE; 2018. p. 1–8. 143

[19] Kumaravel S, et al. Ultra-voltage gain bidirectional dc–dc converter with reduced switch voltage stress and improved efficiency. IEEE Transactions on Circuits and Systems II: Express Briefs. 2022;69(11):4468–4472. 147, 151

[20] Rodríguez-Lorente A, Barrado A, Calderón C, Fernández C, Lázaro A. Non-inverting and non-isolated magnetically coupled buck–boost bidirectional DC–DC converter. IEEE Transactions on Power Electronics. 2020;35(11):11942–11954. 147, 151

[21] Yu L, Wang L, Yang C, Zhu L, Gan Y, Zhang H. A novel nonisolated GaN-Based bidirectional DC–DC converter with high voltage gain. IEEE Transactions on Industrial Electronics. 2021;69(9):9052–9063. 147, 151

[22] Jayaram N, Halder S, Panda KP, Pulavarthi SVK, Arandhakar S, Shankar YR, et al. An Ultra-High Gain Compact Module Bidirectional DC–DC Converter for Energy Storage System. IEEE Access. 2023;11:134023–134039. 147, 151

[23] Wang F, Wang Y, Su B, Teng C. Three-phase interleaved high step-up bidirectional DC–DC converter. IET Power Electronics. 2020;13(12):2469–2480. 147, 151